



Encoding with a fluorescence-activating and absorption-shifting tag generates living bacterial probes for mammalian microbiota imaging



Zhenping Cao¹, Lu Wang¹, Rui Liu, Sisi Lin^{***}, Feng Wu^{**}, Jinyao Liu^{*}

Shanghai Key Laboratory for Nucleic Acid Chemistry and Nanomedicine, Institute of Molecular Medicine, State Key Laboratory of Oncogenes and Related Genes, Shanghai Cancer Institute, Renji Hospital, School of Medicine, Shanghai Jiao Tong University, Shanghai, 200127, China

ARTICLE INFO

Keywords:

Fluorescence-activating
Absorption-shifting
Bacteria
Gut microbiota
Tumor
Imaging

ABSTRACT

The mammalian microbiota plays essential roles in health. A primary determinant to understand the interaction with the host is the distribution and viability of its key microorganisms. Here, a strategy of encoding with a fluorescence-activating and absorption-shifting tag (FAST) is reported to prepare living bacterial probes for real-time dynamic, dual-modal, and molecular oxygen-independent imaging of the host microbiota. Carrying FAST endows bacteria with rapid on-demand turn on-off fluorescence by adding or removal of corresponding fluorophores. Encoded bacteria are able to reversibly switch emission bands for dual-color fluorescence imaging via fluorogen exchange. Due to molecular oxygen-independent emission of FAST, encoded bacteria can emit fluorescence under anaerobic environments including the gut and tumor. These living probes demonstrate the applicability to quantify the vitality of bacteria transplanted to the gut microbiota. This work proposes a unique fluorescence probe for investigating the dynamics of the host microbiota.

1. Introduction

The mammalian microbiota, which exists in different organs or tissues including the skin, gut, lung, eyes, and ears, represents a huge community of microorganisms that plays critical roles in immune modulation and homeostasis maintenance [1–4]. Microorganisms are also able to inhabit various disease sites, for example, inflamed or tumor tissues, forming pathogenic microflora [5,6]. Recently, increasing evidences have proved that the microbiota performs extremely important roles in the host health [7–10]. Disturbance in normal microbiome has been associated with a variety of diseases, such as diabetes, obesity, hypertensive heart disease, inflammatory bowel disease, and some cancers [11–14]. With the development of microbial sequencing technology, both commensal and pathogenic microbes can be analyzed qualitatively and quantitatively, which are instructive for the diagnosis, prevention, and treatment of disease [15,16]. Despite its high throughput and precision, genome sequencing is difficult to track target microflora in manners of dynamic and visual, leading to limited information regarding the distribution and activity of key microbes within the microbiota. Indeed, this information is crucial for understanding the interaction of

the microbiota with its host [17]. Therefore, probes capable of real-time labelling are highly desirable for microbial imaging and analysis.

A number of methods, for instance, the use of chemiluminescence-based molecules or nano-probes as well as the expression of imageable proteins via genetic engineering strategies, have been reported for microbial labelling [18–21]. Benefiting from the flexibility in structural design and fabrication, chemical labelling turns to a widely used method for bacterial marking, particularly the employment of D-amino acid-based metabolic probes to label peptidoglycan in bacterial cell walls [22–24]. Other fluorescent dyes mainly refer to traditional cell membrane and nucleus staining agents that are capable of specifically labelling bacterial membrane or intracellular DNA [25–27]. However, existing methods using chemical labelling are unable to retain consistent fluorescence signal during bacterial proliferation due to the dilution of dyes [28]. The introduced linkers or reactive groups for chemical labelling at specific sites can cause potential cytotoxicity to bacteria [29,30]. Genetic engineering, which endows bacteria with inductively or spontaneously expressed imageable proteins, such as fluorescence proteins and gas vesicle proteins, is an elegant approach to solve these limitations [31–34]. Representatively, as one of fluorescent proteins, green

* Corresponding author.

** Corresponding author.

*** Corresponding author.

E-mail addresses: sisilinjy@outlook.com (S. Lin), wufeng199001@163.com (F. Wu), jyliu@sytu.edu.cn (J. Liu).

¹ These authors contributed equally to this work.

fluorescent protein (GFP) provides a simple yet robust way to genetically tag proteins of interest in bacteria [35,36]. Although the revolutionary significance in cell labelling, fluorescent protein probes suffer from several inherent defects [37,38]. First, fusion process may result in protein dysfunction depending on the size of fluorescent proteins and the fusion site of target proteins [39]. Second, a relatively long period of time is required for fluorophore maturation of fluorescent proteins [40,41]. Third, fluorescent proteins solely emit in the presence of molecular oxygen, meaning that they are incapable of applying in anaerobic conditions such as the microenvironments of gastrointestinal (GI) tract and tumor tissue [42]. Lastly, the signal of fluorescent proteins is fixed and unsuitable for dynamic and multimodal labelling of the host microbiota.

Here, a strategy of encoding with reversible on-off and emission-switchable fluorescence is described to develop living bacterial probes for real-time dynamic and dual-modal imaging of the mammalian microbiota. We encode bacteria with a fluorescence-activating and absorption-shifting tag (FAST), a small protein with a size of 14 kDa, which is evolved from photoactive yellow protein via mutations in several positions [43,44]. Carrying FAST not only possesses typical merits of genetic engineering-based labelling, but also enables a few unique characteristics: 1) prompt on-demand turn on-off fluorescence by binding with or unbinding from specific fluorogens; 2) dynamically reversible switching between different distinguishable emission bands for dual modal imaging through exchanging fluorogens; 3) wide

application of fluorescence imaging in both aerobic and anaerobic environments as the emission of FAST is molecular oxygen independent [45]. As a proof-of-concept study, FAST is transformed into a well-known probiotic bacterium, *Escherichia coli* Nissle 1917 (EcN) [46,47], to prepare living bacterial probes (termed as EcN-FAST, Fig. 1a). In two mouse models of gut and tumor localization, we demonstrate the advantages of intelligent labelling and dual fluorescence modality toward the utilization of EcN-FAST for *in vivo* imaging under anaerobic conditions (Fig. 1b). We show the applicability of FAST-mediated living probes to assess the viability of bacteria transplanted to the gut microflora. Given the maturity of genetic engineering [48], encoding with FAST is anticipated as a versatile approach to prepare various living bacterial probes, offering a platform to disclose the relationship between the mammalian microbiota and its host.

2. Materials and methods

2.1. Materials and strains

Escherichia coli Nissle 1917 strain was purchased from China general microbiological culture collection center (GMCC, China). Plasmids pBBR1MCS2-Tac-mCherry (Kanamycin resistant) and pBBR1MCS2-Tac-eGFP (Kanamycin resistant), and all other reagents were purchased from domestic suppliers and used as received. FAST applied in this work

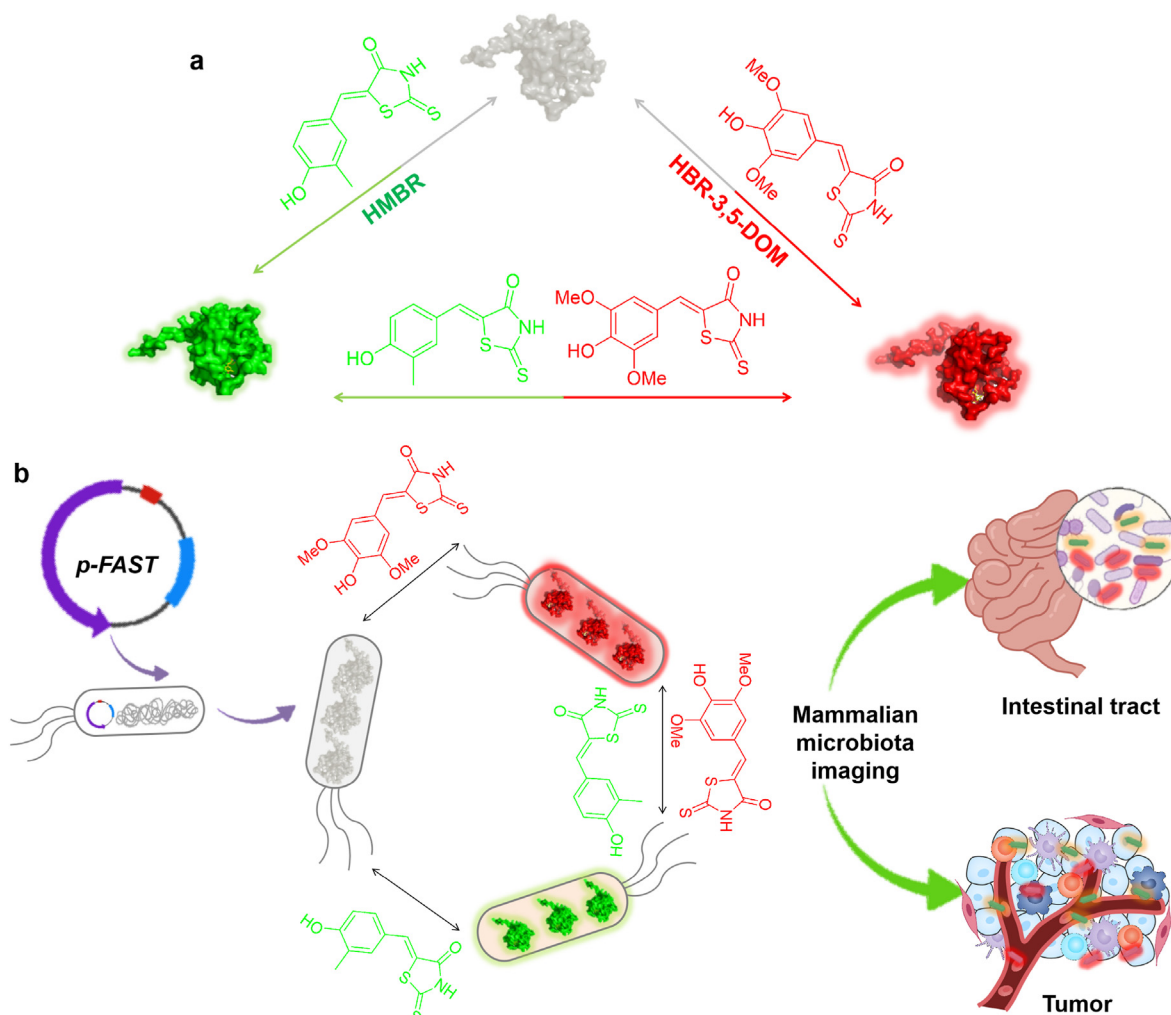


Fig. 1. Schematic illustration of mammalian microbiota imaging by FAST-encoded living bacterial probes. **a** Emission characteristics of FAST. **b** Preparation of EcN-FAST and their applications for real-time dynamic, dual-modal, and molecular oxygen-independent imaging of microbiota associated with the intestinal tract and tumor.

is a variant of mutated photoactive yellow protein (PYP). The plasmids pQE-FAST (Ampicillin resistant) for FAST expression in EcN was constructed by using the *fast* gene template and tagged with a poly-histidine tag (His) [43]. All the bacteria were grown in Luria Bertani (LB) medium at 37 °C with suitable antibiotics. The plasmid containing the *fast* gene template together with 4-hydroxy-3-methylbenzylidene rhodanine (HMBR, green fluorogenic dye) and 4-hydroxy-3,5-dimethoxybenzylidene rhodanine (HBR-3,5-DOM, red fluorogenic dye) were kindly gifted by Dr. Cheng Li and Prof. Arnaud Gautier [43,49].

2.2. Western blot

EcN carrying empty vector and EcN with FAST-His expression vector were cultured overnight and resuspended in phosphate buffered saline (PBS). Cells were mixed with loading buffer and boiled for 5 min. After centrifuging to remove undissolved pellet, 10 µl of each sample was loaded and run on 12% sodiumdodecylsulfate-polyacrylamide gel electrophoresis (SDS-PAGE) gel. The separated samples were transferred onto polyvinylidene difluoride (PVDF) membranes by Bio-rad semi-dry transfer turbo using the preprogrammed protocol for 1.5 mm gel: 1.3 A, 25 V for 10 min (Bio-Rad, USA). The PVDF membrane was incubated in TBS/Tween with 5% skim milk at room temperature for 1 h, followed by incubating with Horseradish Peroxidase (HRP)-conjugated-anti-His antibody (1:5000, AE028, ABclonal, China). The resultant membrane was then incubated with 1 ml enhanced chemiluminescence (ECL) solution for 1 min and captured by a chemiluminescence imager (Bio-rad, USA).

2.3. Turn on in vitro

EcN carrying pQE-FAST were cultured in LB medium with supplement of ampicillin and isopropyl-beta-D-thiogalactopyranoside (IPTG) at 37 °C for 12 h. Bacterial cells were harvested and washed with PBS before incubating with HMBR and HBR-3,5-DOM at room temperature. Fluorescence emission spectra were measured by a fluorospectrometer. The activated EcN-FASTs were imaged by laser scanning confocal microscope (LSCM) through eGFP or mCherry channel and analyzed by flow cytometry using fluoresceine isothiocyanate (FITC) or phycoerythrin (PE).

2.4. Turn-off in vitro

EcN expressing FAST were harvested and incubated with green and red fluorogenic dyes at room temperature for several minutes to activate FAST fluorescence fully. In order to turn off FAST by removing fluorogens, pre-activated EcN-FASTs were resuspended in PBS and washed for a few times. The dynamic turn-off process was visualized by LSCM and analyzed by flow cytometry. The fluorescence intensities of green and red FAST from bacterial cells after washing with PBS for indicated times were recorded by a microplate reader.

2.5. Reversibility in vitro (green to red)

After culture at 37 °C for 12 h with addition of IPTG, EcN expressing FAST were pre-activated by HMBR for several minutes. The green EcN-FAST were fixed on agarose pad and imaged by LSCM as the start point. In order to observe the reversibility of FAST from green to red, 4 µl of red fluorogen HBR-3,5-DOM was added at one side of the agar pad and the same field was continuously captured by both GFP and mCherry channels until green fluorescence disappeared. In addition, the reversibility was analyzed by measuring green and red fluorescence intensities. EcN-FAST was pre-activated by green fluorogen in advance and resuspended in PBS for fluorescence detection, which was indicated as fluorogen exchange time 0. Green EcN-FAST were collected by centrifuge and resuspended into fresh PBS that contains red fluorogen at a higher concentration. Being co-incubated with red fluorogen for a while at 37 °C,

both green and red fluorescence intensities were separately recorded by a microplate reader, indicating as fluorogen exchange times 2. All these procedures were repeated until the elimination of green fluorescence.

2.6. Reversibility in vitro (red to green)

EcN expressing FAST were activated by red fluorogen HBR-3,5-DOM for several minutes after culture at 37 °C for 12 h with addition of IPTG. The red EcN-FAST were fixed on agarose pad and imaged by LSCM as the start point. To observe the reversibility of FAST from red to green, 4 µl of green fluorogen HMBR was added at one side of the agar pad and the same field was continuously captured by both GFP and mCherry channels until red fluorescence disappeared. Furtherly, the reversibility was analyzed by measuring green and red fluorescence intensities. EcN-FAST were firstly incubated with red fluorogen for activation. Green fluorogen in a higher concentration was added into PBS suspension of pre-activated red EcN-FAST and co-incubated at 37 °C shortly. Cells were washed with fresh PBS before the green and red fluorescence intensities of EcN-FAST were separately recorded using a microplate reader.

2.7. Distinguishability of FAST from GFP/mCherry in vitro

HMBR pre-activated EcN-FAST were mixed with EcN expressing GFP (EcN-GFP), fixed on agarose pad, and then observed by LSCM. After focused on a certain view, red fluorogen was added at one side of agarose pad and spread to the other side eventually. During the fluorogen spreading time, the color changing of green EcN-FAST in the certain view was observed. In contrast, the mixture of red EcN-FAST and EcN expressing mCherry (EcN-mCherry) was observed after addition of green fluorogen for separating red EcN-FAST from EcN-mCherry. The dynamic processes were imaged by LSCM and further analyzed by flow cytometry.

2.8. Turn-on of EcN-FAST in anaerobic GI tract

Female ICR mice in 6–8 weeks were purchased from Shanghai Jiesijie laboratory animal company (Shanghai, China) and bred under specific-pathogen-free (SPF) conditions. All animal experiments were performed under the guidelines evaluated and approved by the ethics committee of Institutional Animal Care and Use Committee of Shanghai Jiao Tong University. Each ICR mouse was orally administrated with 1×10^8 colony forming units (CFUs) of EcN-FAST 1 h before gavage of green fluorogen (100 µl). The mice were euthanatized at 1, 2, 4, 8, and 24 h post-administration of green fluorogen, respectively. The entire intestinal tract was extracted and imaged by in vivo imaging system (IVIS) through GFP channel. The fluorescence intensity of each intestinal tract was also recorded.

2.9. Turn-on of EcN-FAST in tumor site

Experiments were performed on female nude BALB/C mice (6–8 weeks) purchased from Shanghai Jiao Tong University School of Medicine (Shanghai, China) and bred under SPF conditions for 4 days. All animal protocols were approved by the Institutional Animal Care and Use Committee guidelines of Shanghai Jiao Tong University School of Medicine. The breast tumor cells (4T1) were collected and resuspended in PBS. 100 µl of PBS containing 5×10^5 of tumor cells was subcutaneously injected into the right flank. After tumor size reaching 1000 mm³, 1×10^7 CFUs of EcN producing FAST were injected into the tumor site of each mouse, followed by injection of 50 µl green fluorogen 1 h post administration of bacteria. The imaging of 4T1 tumor-bearing mice was performed at 0, 3, 6, and 24 h post-intratumor injection of green fluorogen by IVIS through GFP channel.

2.10. Reversibility in the GI tract

Each Institute of Cancer Research (ICR) mouse was fed with 1×10^8

CFUs of green EcN-FAST that were activated by green fluorogen. Red fluorogen was supplied orally 3 h later. The mice were euthanatized at 0.5, 1, 2 and 4 h post-intratumor injection of fluorogen and the GI tract was sectioned for IVIS measurement through both GFP and mCherry channels.

2.11. Reversibility in tumor tissue

After EcN-FAST were activated in tumor site by green fluorogen injection, red fluorogen was injected into tumor site for FAST reversibility test. IVIS measurement of the tumor in each mouse was performed at 3, 6, and 24 h post-administration of red fluorogen through both GFP and mCherry channels. The green and red fluorescence intensities were also recorded by IVIS.

2.12. Quantitative analysis of the viability of EcN-FAST by fluorescence imaging

EcN-FAST were cultured for 12 h and diluted to a serial of concentrations (10^4 , 10^5 , 10^6 , 10^7 , 10^8 and 10^9 CFUs per milliliter). Equivalent fluorogen was added into bacterial solutions for living probe activation before measurement of fluorescence intensity. The relationship between bacterial CFU and fluorescence intensity was recorded by a microplate reader. To test the quantitative capability in the GI tract, 10^7 , 10^8 and 10^9 CFUs of EcN-FAST were orally administrated in female ICR mice (6–8 weeks), following by fluorogen supplement for FAST activation. All the mice were euthanatized 4 h post-administration of green fluorogen for sampling the intestine, which was further imaged by IVIS. After recording the fluorescent intensity, the contents sampled from the stomach, intestine, colon, and cecum were serially diluted with PBS and

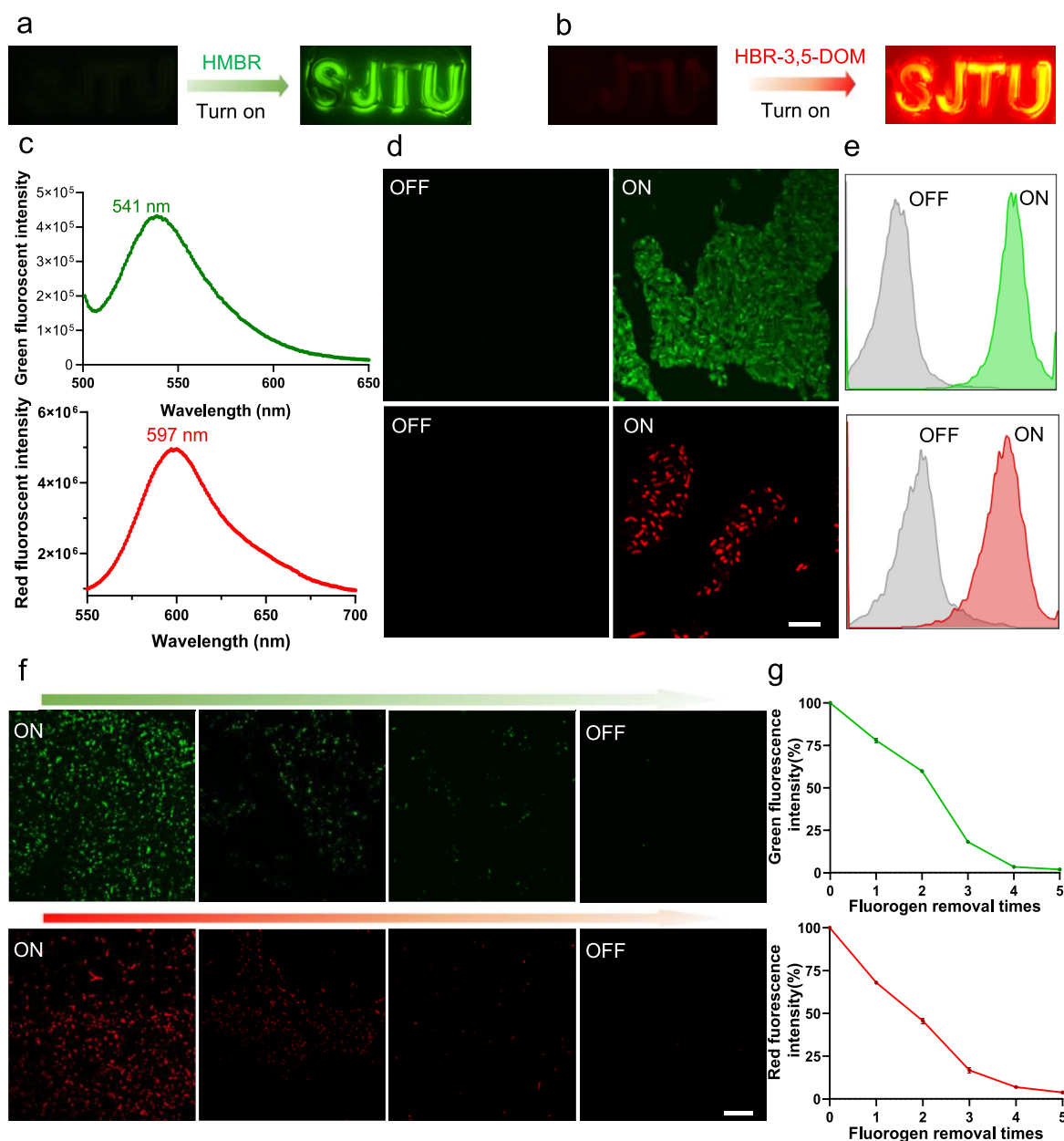


Fig. 2. In vitro on-demand fluorescence turn on-off. **a, b** Fluorescence images of EcN-FAST with or without addition of (a) HMBR and (b) HBR-3,5-DOM. **c** Emission spectra of EcN-FAST after binding with corresponding fluorogens. **d, e** Results of (d) LSCM imaging and (e) flow cytometric analysis of EcN-FAST with or without addition of 20 μ M fluorogens. Scale bar: 10 μ m **f** LSCM imaging of pre-activated EcN-FAST after fluorogen removal with PBS for the indicated times. Scale bar: 10 μ m **g** Relationships between mean fluorescence intensity of EcN-FAST and corresponding fluorogens removal times.

then 50 μ l of each dilution was spread onto solid LB agar plates for 24 h culture before EcN-FAST in the intestinal tract were counted. The linear regression analysis was performed by Microsoft Excel.

3. Results and discussion

3.1. Design, preparation and fluorescence turn on-off of EcN-FAST

Given the merits of biosynthetic technology, bacteria have been broadly engineered to construct living materials that can be applied in different fields, such as diagnostics, 3D printing, and environment remediation [50–53]. Due to their natural behaviors of proliferation and colonization in the host, bacteria expressing fluorescence proteins can be explored as living fluorescence probes for tracking the interactions between the microbiota and its host [54]. To generate encoded bacteria, FAST was fused with a His-tag and co-expressed in EcN. As confirmed in

Fig. S1, FAST-His was detected by western blot via HRP conjugated mouse anti-His-tag monoclonal antibody, suggesting that FAST was successfully expressed in EcN. Two fluorogens of HMBR and HBR-3,5-DOM, which were stable in physiologically relevant conditions [43, 49], were used to specifically bind with FAST. To validate on-demand fluorescence turn-on, a cytocompatible concentration of 20 μ M of HMBR was supplied into EcN-FAST culture [55], showing a significant increment in green fluorescence signal compared to EcN carrying empty vector upon excitation at 488 nm (Fig. 2a and b, Fig. S2). Similar to HMBR, an immediate increase of red fluorescence was observed once adding HBR-3,5-DOM, which in turn reflected the normal function of homologous FAST to bind with corresponding fluorogens in recombinant EcN. Emission max of HMBR and HBR-3,5-DOM was found to be 541 and 597 nm, respectively (Fig. 2c). Fluorescence turn-on of EcN-FAST was further visualized via confocal microscopy, displaying fluorescently activated bacteria following the addition of HMBR or HBR-3,5-DOM

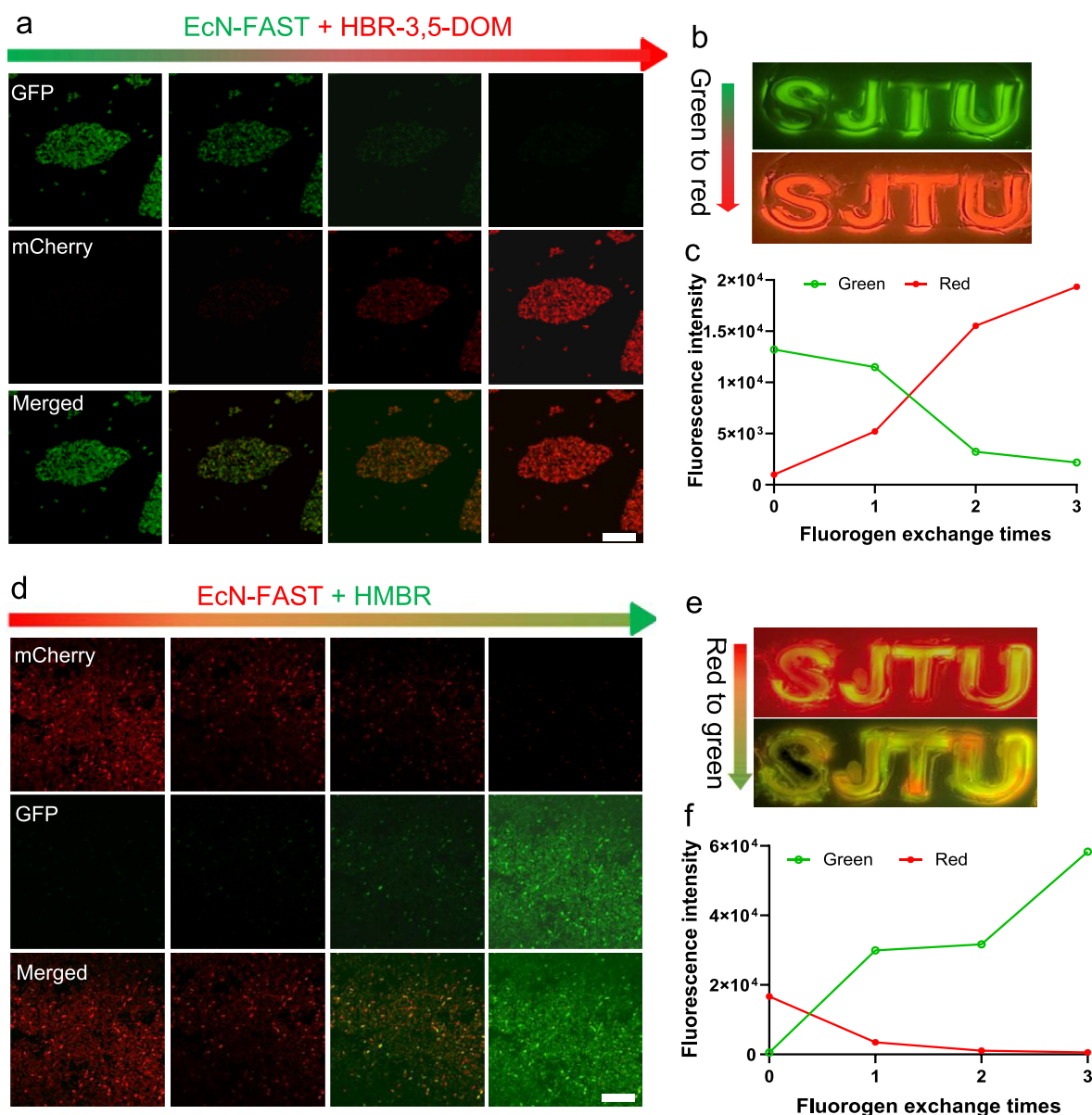


Fig. 3. Reversible switch of emission bands in vitro. **a** Typical LSCM images of HMBR-activated EcN-FAST after adding HBR-3,5-DOM. Scale bar, 10 μ m **b** Fluorescence switch by replacing HMBR with HBR-3,5-DOM. **c** Relationship of fluorescence intensity after rinsing HMBR-activated EcN-FAST with PBS solution of HBR-3,5-DOM for the indicated times. **d** LSCM images of HBR-3,5-DOM-activated EcN-FAST after adding HMBR. Scale bar, 10 μ m **e** Fluorescence switch by replacing HBR-3,5-DOM with HMBR. **f** Relationship of fluorescence intensity after rinsing HBR-3,5-DOM-activated EcN-FAST with PBS solution of HMBR for the indicated times. Error bars represent standard deviation ($n = 3$).

(Fig. 2d). Flow cytometric analysis was performed and histograms shown in Fig. 2e also verified a large shift of individual bacterial fluorescence to the higher intensity after complexing with HMBR or HBR-3,5-DOM. In consideration of that the fluorescence intensity of FAST directly depends on fluorogen concentration [37], we speculated that the emission of bacteria could be turned off as needed by removing the bound fluorogens. To prove this hypothesis, fluorescently activated EcN-FAST were repeatedly resuspended in PBS to remove bound fluorogens gradually. The intensity of bacteria fluorescence was measured by LSCM, flow cytometry, and fluorescence microplate reader after each resuspension. Representative confocal images showed that the signal of EcN-FAST diminished with increasing rinsing times (Fig. 2f). This was ascribed to the dissociation between FAST and HMBR/HBR-3,5-DOM caused by the dilution of fluorogens. Consistent with the result of confocal imaging, flow cytometry analysis also demonstrated fluorescent fading of EcN-FAST with resuspension increasing from 1 to 5 times (Fig. 2g and Fig. S3).

3.2. Reversible switch of emission bands

Having testified reversible on-off fluorescence of EcN-FAST, we turned our attention to investigate whether the emission bands could be distinguishably switched for dual modal imaging in light of dynamic emission behavior of FAST. To validate this possibility, EcN-FAST fluorescently pre-activated by green fluorogen of HMBR were added with red fluorogen of HBR-3,5-DOM. The variation of fluorescence emission was captured by LSCM. As shown in Fig. 3a and b, with increasing the concentration of HBR-3,5-DOM from 10 to 50 μM , the signal of green fluorescence of EcN-FAST decreased continuously and no detectable fluorescence signal was observed eventually. In the meantime, red fluorescence signal increased with HBR-3,5-DOM concentration under the same experimental conditions. Co-localization analysis in fluorescence microscopy indicated a distinguishable switching of emission bands by replacing HMBR with HBR-3,5-DOM. The switching of emission was further quantified by a microplate reader, presenting a near complete disappearance of green fluorescence signal, while a significant enhancement of red fluorescence intensity was obtained during the same period of time (Fig. 3c). The dynamic variation of fluorescence emission was attributed to that higher HBR-3,5-DOM concentration could promote the dissociation of bound HMBR via competing for complexation with FAST in bacteria. On the contrary, bacteria fluorescently pre-activated by

red fluorogen of HBR-3,5-DOM were supplemented with green fluorogen of HMBR. As expected, similar emission switching was procured for EcN-FAST, as supported by the results of fluorescence imaging and quantification analysis, approaching a full conversion of emission from red to green fluorescence (Fig. 3d–f). Briefly, all these results pointed out that the emission bands of encoded bacteria could be distinguishably switched in a dynamical and reversible fashion, demonstrating the suitability of EcN-FAST for dual modal imaging.

In view of its dual modality of fluorescence emission, we then evaluated the capacity of FAST labelling to avoid fluorescence interference to identify encoded bacteria from the microbiota. For this purpose, a fluorescence crosstalk model was designed by mixing EcN-FAST with EcN-GFP. After exposure to excitation at 488 nm, both EcN-GFP and HMBR pre-activated EcN-FAST displayed similar emission, as reflected by sole green fluorescence signal under confocal imaging (Fig. 4a). Under this circumstance, the identification of encoded bacteria was interrupted by fluorescence crosstalk. With the addition of HBR-3,5-DOM, a portion of these fluorescent bacteria switched their emission from green to red fluorescence signal, which was resulted from the exchange of fluorogen. As further supported in Fig. 4b, flow cytometry histograms claimed the elimination of emission at 541 nm together with an emergence of striking emission at 597 nm. Namely, the dual imaging modality of FAST enabled a distinction between encoded EcN and other bacteria even carrying interferential fluorescence signals. Furthermore, another crosstalk model was developed by mixing EcN-FAST with EcN-mCherry. At this point, both EcN-mCherry and HBR-3,5-DOM pre-activated EcN-FAST glowed red fluorescence signal after irradiation (Fig. 4c). Expectedly, once supplementation with HMBR, a certain number of bacteria turned to green fluorescence, meaning the replacement of HBR-3,5-DOM in the pre-activated EcN-FAST. Fluorogen exchange mediated emission switching was also affirmed by reversed shift of flow cytometry histograms following the addition of HMBR (Fig. 4d). Distinct from fluorescently unchangeable GFP and mCherry, the tunability and reversibility of FAST conferred encoded EcN with feasibility to visualize the distribution of bacteria of interest among the host microbiota.

3.3. In vivo imaging under anaerobic environments

Encouraged by the in vitro performances, we next assessed the fluorescence labelling of EcN-FAST located in anaerobic in vivo environments including the GI tract and tumor. The gut microbiota, a wide

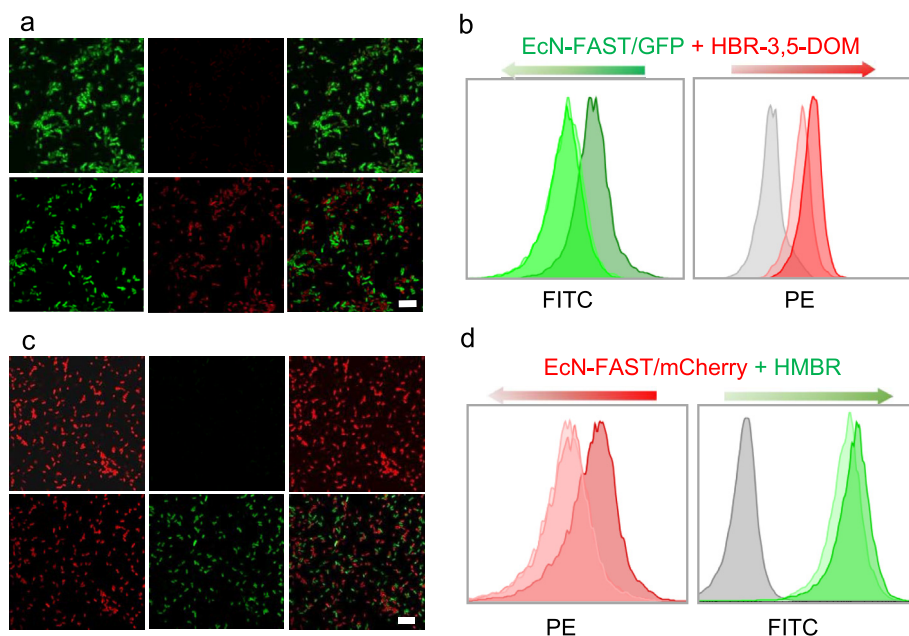


Fig. 4. Distinguishability of EcN-FAST in vitro. **a** LSCM images of the mixture of HMBR-activated EcN-FAST and EcN expressing GFP with or without the addition of HBR-3,5-DOM. Scale bar: 10 μm **b** Flow cytometry histograms of HMBR-activated EcN-FAST in the mixture with or without supplementation with HBR-3,5-DOM. **c** LSCM images of the mixture of HBR-3,5-DOM-activated EcN-FAST and EcN expressing mCherry with or without the addition of HMBR. Scale bar: 10 μm **d** Flow cytometry histograms of HBR-3,5-DOM-activated EcN-FAST in the mixture with or without supplementation with HMBR.

variety of symbiotic bacteria as well as other microbes that inhabit the GI tract, has been recognized as an important modulator in human health [56]. Investigating the colonization distribution of a specific bacterial strain within the gut microbiota is a key step toward the disclosure of mutual interaction between the microbiota and its host [54]. In a mouse model, 1×10^8 CFUs of EcN-FAST were gavaged, followed by oral ingestion of 100 μ l of 5 mM HMBR. At the indicated time points, the intestinal tract was sampled and intraluminal distribution of EcN-FAST was imaged by IVIS. IVIS images in Fig. 5a presented that EcN-FAST were able to emit inside anaerobic intraluminal environment of the intestinal tract after supplementing with HMBR. With the increase of time post-administration, orally delivered EcN colonized the intestine sufficiently, as implied by rapid bacterial proliferation that was confirmed by greatly enhanced fluorescence intensity. It was found that the colonization of EcN in the intestine reached a peak value around 8 h after oral

gavage and then decreased with time (Fig. 5b). We also studied the property of in vivo imaging by detecting the dual fluorescence modality of EcN-FAST in the gut. Each mouse was fed with 1×10^8 CFUs of HMBR pre-activated EcN-FAST 3 h before applying HBR-3,5-DOM by gavage. Both fluorescence imaging and quantified signal intensity acquired by IVIS depicted that the emission of FAST-HMBR reduced, while the intensity of fluorescence associated with FAST-HBR-3,5-DOM strengthened evidently (Fig. 5c and d). The simultaneous presence of dual fluorescence signal proposed the capability of EcN-FAST for double-mode imaging.

In addition, we characterized the labelling of EcN-FAST localized inside hypoxic tumor tissue considering that genome sequencing has recently highlighted the existence of intratumoral microbiota as well as its importance in tumor progression and regression [16]. In a murine model of 4T1 breast tumor, 1×10^7 CFUs of EcN-FAST were injected intratumorally, followed by an intratumoral injection of HMBR. IVIS

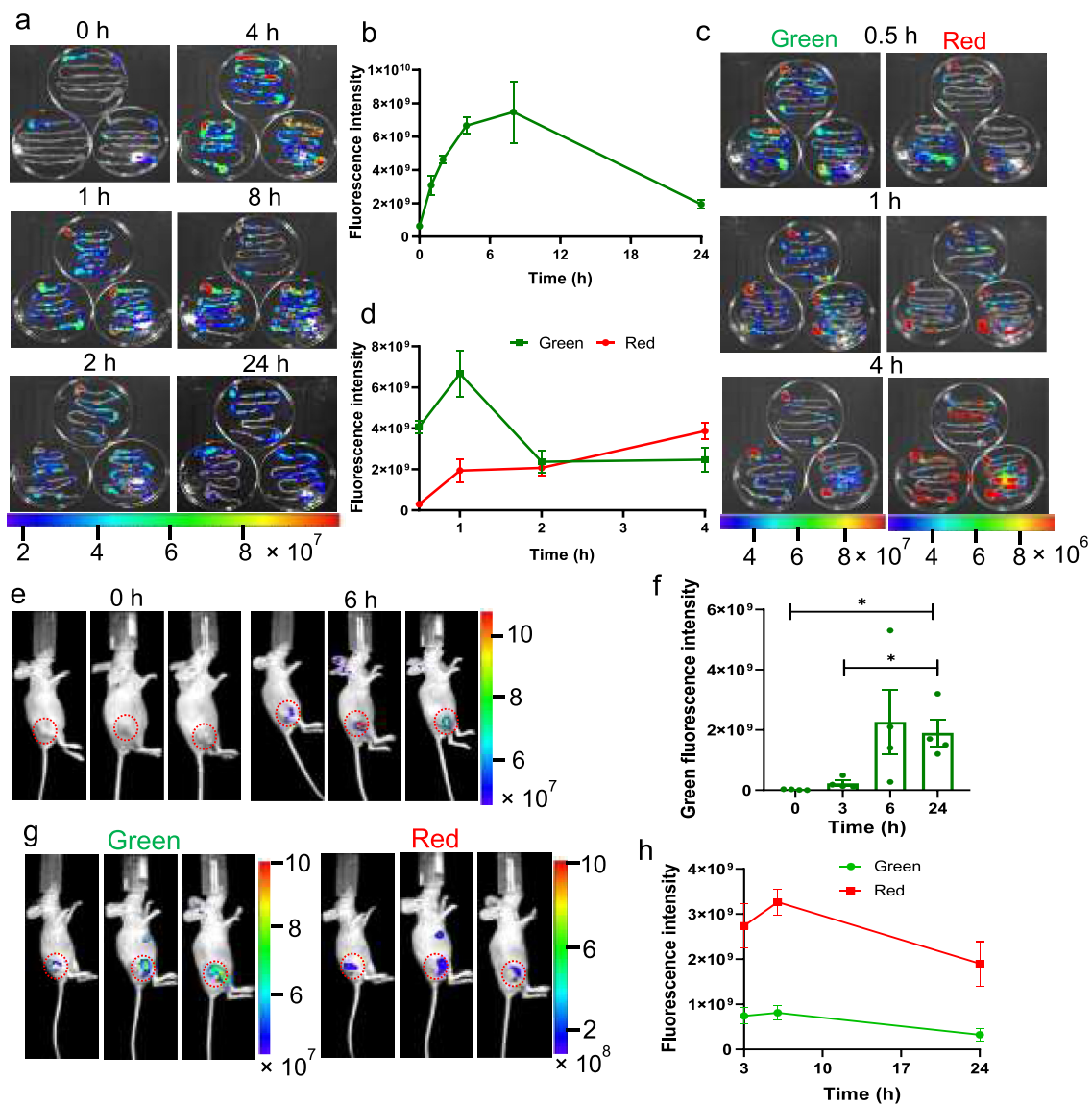


Fig. 5. In vivo imaging under anaerobic environments. **a** IVIS images of the intestinal tracts sectioned from mice treated with EcN-FAST and HMBR. **b** Fluorescence intensity of EcN-FAST in the intestinal tract after HMBR supplementation. **c** IVIS images of the intestinal tracts sampled from mice dosed with HMBR-activated EcN-FAST and HBR-3,5-DOM. **d** Fluorescence intensity of HMBR-activated EcN-FAST in the intestinal tract after adding with HBR-3,5-DOM. Error bars represent standard deviation. **e** IVIS images of mice after intratumoral injection with EcN-FAST and HMBR. **f** Fluorescence intensity of EcN-FAST in tumor site after adding HMBR. **g** IVIS images of mice after intratumoral administration with HMBR-activated EcN-FAST and HBR-3,5-DOM. **h** Fluorescence intensity of HMBR-activated EcN-FAST in tumor site after adding HBR-3,5-DOM. HMBR: λ_{ex} 488 nm, λ_{em} 510 nm; HBR-3,5-DOM: λ_{ex} 587 nm, λ_{em} 610 nm. Error bars represent the standard deviation ($n = 3-4$). Significance was assessed using Student's *t*-test, giving *p* values, $p < 0.05$, *. Scale bar in IVIS image refers to radiance ($p/s/cm^2/sr$).

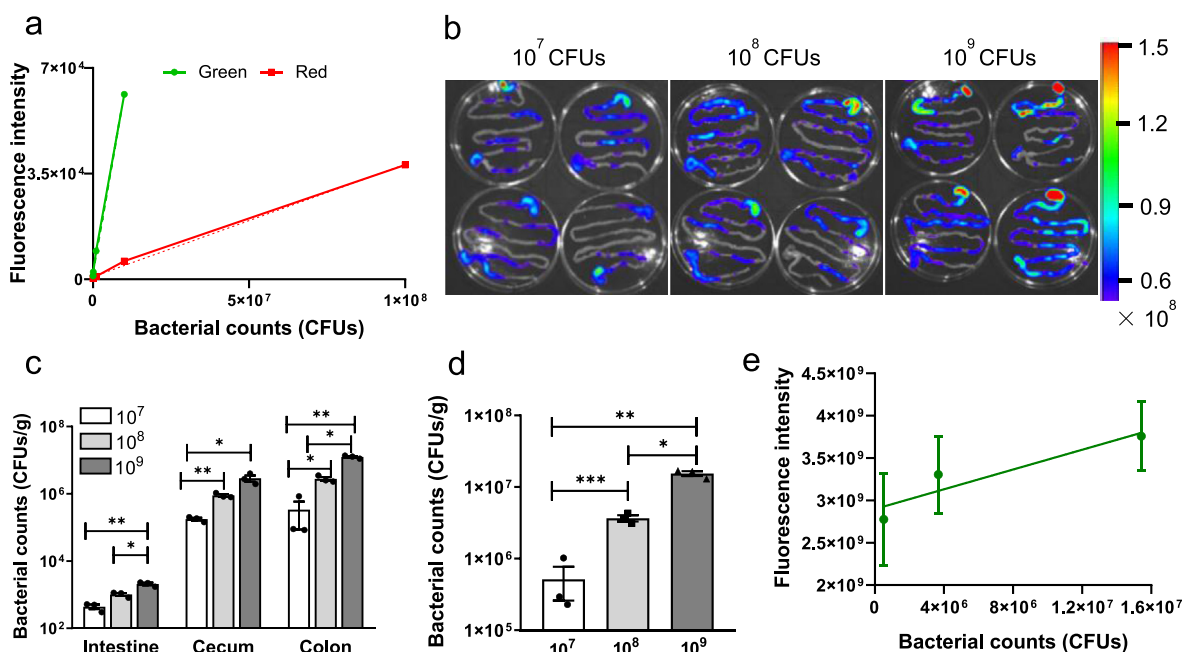


Fig. 6. Quantification of in vivo bacterial viability by EcN-FAST. **a** Relationship between the intensity of FAST fluorescence and the CFUs of EcN-FAST. **b** IVIS images of the intestinal tracts sampled from mice orally gavaged with the indicated amounts of EcN-FAST and HMBR. **c** Numbers of EcN-FAST in the intestine, colon, and cecum quantified by plate counting. **d** Total amounts of EcN-FAST retaining in the intestinal tract. **e** Relationship between fluorescence intensity of HMBR-activated EcN-FAST and the count of EcN-FAST in the intestine tract. Error bars represent standard deviation ($n = 3-4$). Significance was assessed using Student's *t*-test, giving *p* values, $p < 0.05$, *; $p < 0.01$, **; $p < 0.005$, ***. Scale bar in IVIS image refers to radiance ($\text{p/s/cm}^2/\text{sr}$).

imaging together with quantitative analysis illustrated that EcN-FAST could colonize tumor site, with the appearance of a maximum fluorescence intensity 6 h post injection (Fig. 5e and f). Different from the intestinal tract, transplanted bacteria exhibited continuous tumor colonization, as suggested by a comparable signal intensity observed even with time prolonging to 24 h. The adequate residence of EcN-FAST could be resulted from the nutritious and immunosuppressive tumor microenvironment [57]. Similarly, upon injection with HBR-3,5-DOM, mice colonized with HMBR pre-activated EcN-FAST emerged fluorescence signal of FAST-HBR-3,5-DOM, displaying dual color chromogenic tumors (Fig. 5g and h). Taken together, these data clarified the intelligence and dual-modality of encoded bacteria for fluorescence imaging in anaerobic in vivo environments of the gut and tumor.

3.4. Potential application of EcN-FAST

We further explored the applicability of encoded bacteria to evaluate the activity of bacteria transplanted to the gut microbiota. The transplantation of beneficial bacteria to the gut microbiome, including oral microecology and fecal microbiota transplantation, has been implemented for treating autoimmune disorders, bowel inflammations, metabolic dysfunctions, certain types of cancer, and others [58–60]. Quantitative analysis of bacterial viability is of great significance for understanding the impact of transplanted bacteria on the modulation of the gut microbiota [28]. The ability of EcN-FAST to quantitatively analyze bacterial vitality was appraised by both in vitro and in vivo assessments. EcN-FAST were cultured for 12 h and diluted to a serial of incremental CFUs of 10^4 , 10^5 , 10^6 , 10^7 , 10^8 , and 10^9 per milliliter, which were added by $10 \mu\text{l}$ of $50 \mu\text{M}$ HMBR or HBR-3,5-DOM. The measurement of activated fluorescence indicated linearly fitted relationships between bacterial number and fluorescence intensity of EcN-FAST, giving R^2 values of 0.999 and 0.997 for FAST-HMBR and FAST-HBR-3,5-DOM, respectively (Fig. 6a). This result meant that with the help of specific fluorogens, the viability of EcN-FAST could be calculated by recording their fluorescent intensity. To determine the accuracy for in vivo

evaluation of bacterial vitality, 10^7 , 10^8 , and 10^9 CFUs of EcN-FAST were orally delivered into mice and fluorescently activated by HMBR via gavage. The intestinal tract was harvested 5 h post-administration and the overall fluorescence intensity of each sample was recorded by IVIS imaging (Fig. 6b). To examine the relationship with the number of survived bacteria, contents extracted from the intestine, colon, and cecum were serially diluted with PBS and then $50 \mu\text{l}$ of each dilution was spread onto solid LB agar plates for bacterial counting (Fig. 6c). As illustrated in Fig. 6d and e, although passage through harsh and complicated environments of the GI tract, the relation between fluorescent intensity and the number of EcN survived in the intestinal tract was near linear, verifying the value of EcN-FAST for assessing the activity of bacteria within the microbiota.

4. Conclusion

In summary, we report an approach of encoding with a photoactive yellow protein derived tag to prepare living bacterial probes for imaging the mammalian microbiota. In addition to conventional advantages of genetic engineering-mediated labelling, carrying a small FAST protein endows encoded bacteria with several unique characteristics, including sensitive on-demand turn on-off signals by binding with or dissociating from fluorogen of HMBR or HBR-3,5-DOM, dynamically reversible switching between distinguishable emissions at 541 and 597 nm for dual-mode imaging via exchanging corresponding fluorogens, and wide application in both aerobic and anaerobic environments by virtue of molecular oxygen independent emission of FAST. Significantly, these merits are further validated in two murine models of gut and tumor localization. FAST-mediated living probes also demonstrate their applicability to quantitatively analyze the activity of bacteria transplanted to the gut microbiota. Our work provides an innovative bacterial probe to fluorescently image the mammalian microbiota and offers an alternative to study its interaction with the host.

Credit author statement

J.L. supervised the project. J.L. conceived and designed the experiments with Z.C., S.L. and F.W. Z.C., L.W., R.L., S.L. and F.W. performed all experiments. All authors analyzed and discussed the data. Z.C. and J.L. wrote the paper.

Data availability statement

All data needed to evaluate the conclusions in the paper are present in the paper and/or the Supplementary Materials. Additional data related to this paper may be requested from the authors.

Declaration of competing interest

The authors declare that they have no known competing financial interests or personal relationships that could have appeared to influence the work reported in this paper.

Acknowledgements

This work was financially supported by the National Key Research and Development Program of China (SQ2021YFA090162), the National Natural Science Foundation of China (21875135, 32101218, 52101289, 22105123), the Youth Science and Technology Talents Yang Fan Plan of Shanghai (19YF1427800), the Innovative Research Team of High-Level Local Universities in Shanghai (SHSMU-ZDCX20210900, SHSMU-ZDCX20210700), and the Interdisciplinary Program of Shanghai Jiao Tong University (ZH2018QNA44, YG2022QN032).

Appendix A. Supplementary data

Supplementary data to this article can be found online at <https://doi.org/10.1016/j.mtbio.2022.100311>.

References

- Y. Wu, C.Z. Wang, J.Y. Wan, H. Yao, C.S. Yuan, Dissecting the interplay mechanism between epigenetics and gut microbiota: health maintenance and disease prevention, *Int. J. Mol. Sci.* 22 (2021) 6933.
- A. Heintz-Buschart, P. Wilmes, Human gut microbiome: function matters, *Trends Microbiol.* 26 (2018) 563–574.
- K.F. Budden, S.L. Gellatly, D.L. Wood, M.A. Cooper, M. Morrison, P. Hugenholtz, P.M. Hansbro, Emerging pathogenic links between microbiota and the gut-lung axis, *Nat. Rev. Microbiol.* 15 (2017) 55–63.
- X. Li, L. Xing, R. Lai, C. Yuan, P. Humbert, Literature mapping: association of microscopic skin microflora and biomarkers with macroscopic skin health, *Clin. Exp. Dermatol.* 46 (2021) 21–27.
- B.A. Helmink, M.A.W. Khan, A. Hermann, V. Gopalakrishnan, J.A. Wargo, The microbiome, cancer, and cancer therapy, *Nat. Med.* 25 (2019) 377–388.
- F. McAllister, M.A.W. Khan, B. Helmink, J.A. Wargo, The tumor microbiome in pancreatic cancer: bacteria and beyond, *Cancer Cell* 36 (2019) 577–579.
- Y. Fan, O. Pedersen, Gut microbiota in human metabolic health and disease, *Nat. Rev. Microbiol.* 19 (2021) 55–71.
- W.E. Ruff, T.M. Greiling, M.A. Krieger, Host-microbiota interactions in immune-mediated diseases, *Nat. Rev. Microbiol.* 18 (2020) 521–538.
- D. Dodd, M.H. Spitzer, W. Van Treuren, B.D. Merrill, A.J. Hryckowian, S.K. Higginbottom, A. Le, T.M. Cowan, G.P. Nolan, M.A. Fischbach, J.L. Sonnenburg, A gut bacterial pathway metabolizes aromatic amino acids into nine circulating metabolites, *Nature* 551 (2017) 648–652.
- Y.E. Chen, M.A. Fischbach, Y. Belkaid, Skin microbiota-host interactions, *Nature* 553 (2018) 427–436.
- J.L. Alexander, I.D. Wilson, J. Teare, J.R. Marchesi, J.K. Nicholson, J.M. Kinross, Gut microbiota modulation of chemotherapy efficacy and toxicity, *Nat. Rev. Gastroenterol. Hepatol.* 14 (2017) 356–365.
- T. Eom, Y.S. Kim, C.H. Choi, M.J. Sadowsky, T. Unno, Current understanding of microbiota- and dietary-therapies for treating inflammatory bowel disease, *J. Microbiol.* 56 (2018) 189–198.
- M. Knip, H. Siljander, The role of the intestinal microbiota in type 1 diabetes mellitus, *Nat. Rev. Endocrinol.* 12 (2016) 154–167.
- L.H.S. Lau, S.H. Wong, Microbiota, obesity and NAFLD, *Adv. Exp. Med. Biol.* 1061 (2018) 111–125.
- A.H. van Vliet, Next generation sequencing of microbial transcriptomes: challenges and opportunities, *FEMS Microbiol. Lett.* 302 (2010) 1–7.
- E. Riquelme, Y. Zhang, L. Zhang, M. Montiel, M. Zoltan, W. Dong, P. Quesada, I. Sahin, V. Chandra, A. San Lucas, P. Scheet, H. Xu, S.M. Hanash, L. Feng, J.K. Burks, K.A. Do, C.B. Peterson, D. Nejman, C.D. Tzeng, M.P. Kim, C.L. Sears, N. Ajami, J. Petrosino, L.D. Wood, A. Maitra, R. Strausman, M. Katz, J.R. White, R. Jenq, J. Wargo, F. McAllister, Tumor microbiome diversity and composition influence pancreatic cancer outcomes, *Cell* 178 (2019) 795–806.
- H. Shi, Q. Shi, B. Grodner, J.S. Lenz, W.R. Zipfel, I.L. Brito, I. De Vlamincq, Highly multiplexed spatial mapping of microbial communities, *Nature* 588 (2020) 676–681.
- N. Kumar, Y. Hori, K. Kikuchi, Photoactive yellow protein and its chemical probes: an approach to protein labelling in living cells, *J. Biochem.* 166 (2019) 121–127.
- T. Kostic, L. Bodrossy, Sequence-specific end labeling of oligonucleotides (SSELO)-Based microbial detection, *Methods Mol. Biol.* 1918 (2019) 47–56.
- L. Lin, Y. Du, J. Song, W. Wang, C. Yang, Imaging commensal microbiota and pathogenic bacteria in the gut, *Acc. Chem. Res.* 54 (2021) 2076–2087.
- W. Wang, N. Zhang, Y. Du, J. Gao, M. Li, L. Lin, D.M. Czajkowsky, X. Li, C. Yang, Z. Shao, Three-dimensional quantitative imaging of native microbiota distribution in the gut, *Angew. Chem., Int. Ed. Engl.* 60 (2021) 3055–3061.
- E. Kuru, S. Tekkam, E. Hall, Y.V. Brun, M.S. Van Nieuwenhze, Synthesis of fluorescent D-amino acids and their use for probing peptidoglycan synthesis and bacterial growth in situ, *Nat. Protoc.* 10 (2015) 33–52.
- W. Wang, L. Lin, Y. Du, Y. Song, X. Peng, X. Chen, C.J. Yang, Assessing the viability of transplanted gut microbiota by sequential tagging with D-amino acid-based metabolic probes, *Nat. Commun.* 10 (2019) 1317.
- Y.P. Hsu, E. Hall, G. Booher, B. Murphy, A.D. Radkov, J. Yablonowski, C. Mulcahey, L. Alvarez, F. Cava, Y.V. Brun, E. Kuru, M.S. VanNieuwenhze, Fluorogenic D-amino acids enable real-time monitoring of peptidoglycan biosynthesis and high-throughput transpeptidation assays, *Nat. Chem.* 11 (2019) 335–341.
- B. Chazotte, Labeling nuclear DNA using DAPI, *Cold Spring Harb. Protoc.* 1 (2011) pdb prot5556.
- B. Chazotte, Labeling nuclear DNA with hoechst 33342, *Cold Spring Harb. Protoc.* 1 (2011) pdb prot5557.
- F. Kurth, P.S. Dittich, P. Walde, D. Seebach, Influence of the membrane dye R18 and of DMSO on cell penetration of guanidinium-rich peptides, *Chem. Biodivers.* 15 (2018) e1800302.
- W. Wang, Q. Yang, Y. Du, X. Zhou, X. Du, Q. Wu, L. Lin, Y. Song, F. Li, C. Yang, W. Tan, Metabolic labeling of peptidoglycan with NIR-II dye enables in vivo imaging of gut microbiota, *Angew. Chem., Int. Ed. Engl.* 59 (2020) 2628–2633.
- N.K. Olrichs, M.E. Aarsman, J. Verheul, C.J. Arnusch, N.I. Martin, M. Herve, W. Vollmer, B. de Kruijff, E. Breukink, T. den Blaauwen, A novel in vivo cell-wall labeling approach sheds new light on peptidoglycan synthesis in *Escherichia coli*, *Chembiochem* 12 (2011) 1124–1133.
- K. Tiyanont, T. Doan, M.B. Lazarus, X. Fang, D.Z. Rudner, S. Walker, Imaging peptidoglycan biosynthesis in *Bacillus subtilis* with fluorescent antibiotics, *Proc. Natl. Acad. Sci. U.S.A.* 103 (2006) 11033–11038.
- M.M. Karasev, O.V. Stepanenko, K.A. Rumyantsev, K.K. Turoverov, V.V. Verkhusha, Near-infrared fluorescent proteins and their applications, *Biochemistry* 84 (2019) 32–50.
- R.W. Bourdeau, A. Lee-Gosselin, A. Lakshmanan, A. Farhadi, S.R. Kumar, S.P. Nety, M.G. Shapiro, Acoustic reporter genes for noninvasive imaging of microorganisms in mammalian hosts, *Nature* 553 (2018) 86–90.
- C. Xiao, L. Li, L. Lao, Y. Liu, Q. Wei, Q. Ji, G. Sun, F. Lin, J. Wang, G. Bao, Application of the red fluorescent protein mCherry in mycelial labeling and organelle tracing in the dermatophyte *Trichophyton mentagrophytes*, *FEMS Microbiol. Lett.* (2018) 365.
- A. Iyer, M. Baranov, A.J. Foster, S. Chordia, G. Roelfes, R. Vlijm, G. van den Bogaart, B. Poolman, Chemogenetic tags with probe exchange for live-cell fluorescence microscopy, *ACS Chem. Biol.* 16 (2021) 891–904.
- J.D. Pedelacq, S. Cabantous, T. Tran, T.C. Terwilliger, G.S. Waldo, Engineering and characterization of a superfolder green fluorescent protein, *Nat. biotech.* 24 (2006) 79–88.
- M. Chalfie, Green fluorescent protein, *Photochem. Photobiol.* 62 (1995) 651–656.
- M.A. Plamont, E. Billon-Denis, S. Maurin, C. Gauron, F.M. Pimenta, C.G. Specht, J. Shi, J. Querard, B. Pan, J. Rossignol, K. Moncoq, N. Morellet, M. Volovitch, E. Lescop, Y. Chen, A. Triller, S. Vriz, T. Le Saux, L. Jullien, A. Gautier, Small fluorescence-activating and absorption-shifting tag for tunable protein imaging in vivo, *Proc. Natl. Acad. Sci. U.S.A.* 113 (2016) 497–502.
- J. Wiedenmann, F. Oswald, G.U. Nienhaus, Fluorescent proteins for live cell imaging: opportunities, limitations, and challenges, *IUBMB Life* 61 (2009) 1029–1042.
- S. Cabantous, T.C. Terwilliger, G.S. Waldo, Protein tagging and detection with engineered self-assembling fragments of green fluorescent protein, *Nat. biotech.* 23 (2005) 102–107.
- T.D. Craggs, Green fluorescent protein: structure, folding and chromophore maturation, *Chem. Soc. Rev.* 38 (2009) 2865–2875.
- E. Hebisch, J. Knebel, J. Landsberg, E. Frey, M. Leisner, High variation of fluorescence protein maturation times in closely related *Escherichia coli* strains, *PLoS One* 8 (2013), e75991.
- S.J. Remington, Fluorescent proteins: maturation, photochemistry and photophysics, *Curr. Opin. Struct. Biol.* 16 (2006) 714–721.
- C. Li, M.A. Plamont, H.L. Sladitschek, V. Rodrigues, I. Aujard, P. Neveu, T. Le Saux, L. Jullien, A. Gautier, Dynamic multicolor protein labeling in living cells, *Chem. Sci.* 8 (2017) 5598–5605.
- A.G. Tebo, B. Moeyaert, M. Thauvin, I. Carlon-Andres, D. Boken, M. Volovitch, S. Padilla-Parra, P. Dedecker, S. Vriz, A. Gautier, Orthogonal fluorescent chemogenetic reporters for multicolor imaging, *Nat. Chem. Biol.* 17 (2021) 30–38.

- [45] M. Flaiz, G. Ludwig, F.R. Bengelsdorf, P. Durre, Production of the biocommodities butanol and acetone from methanol with fluorescent FAST-tagged proteins using metabolically engineered strains of *Eubacterium limosum*, *Biotechnol. Biofuels* 14 (2021) 117.
- [46] C.A. Jacobi, P. Malfertheiner, *Escherichia coli* Nissle 1917 (Mutaflor): new insights into an old probiotic bacterium, *Dig. Dis.* 29 (2011) 600–607.
- [47] B. Ou, Y. Yang, W.L. Tham, L. Chen, J. Guo, G. Zhu, Genetic engineering of probiotic *Escherichia coli* Nissle 1917 for clinical application, *Appl. Microbiol. Biotechnol.* 100 (2016) 8693–8699.
- [48] J.H. Collins, E.M. Young, Genetic engineering of host organisms for pharmaceutical synthesis, *Curr. Opin. Biotechnol.* 53 (2018) 191–200.
- [49] C. Li, A.G. Tebo, M. Thauvin, M.A. Plamont, M. Volovitch, X. Morin, S. Vriz, A. Gautier, A far-red emitting fluorescent chemogenetic reporter for in vivo molecular imaging, *Angew. Chem., Int. Ed. Engl.* 59 (2020) 17917–17923.
- [50] J. Huang, S. Liu, C. Zhang, X. Wang, J. Pu, F. Ba, S. Xue, H. Ye, T. Zhao, K. Li, Y. Wang, J. Zhang, L. Wang, C. Fan, T.K. Lu, C. Zhong, Programmable and printable *Bacillus subtilis* biofilms as engineered living materials, *Nat. Chem. Biol.* 15 (2019) 34–41.
- [51] Y. Li, K. Li, X. Wang, M. X. M. Cui, P. Ge, J. Zhang, F. Qiu, C. Zhong, Conformable self-assembling amyloid protein coatings with genetically programmable functionality, *Sci. Adv.* 6 (2020) eaba1425.
- [52] Y. Wang, B. An, B. Xue, J. Pu, X. Zhang, Y. Huang, Y. Yu, Y. Cao, C. Zhong, Living materials fabricated via gradient mineralization of light-inducible biofilms, *Nat. Chem. Biol.* 17 (2021) 351–359.
- [53] X. Wang, J. Pu, Y. Liu, F. Ba, M. Cui, K. Li, Y. Xie, Y. Nie, Q. Mi, T. Li, L. Liu, M. Zhu, C. Zhong, Immobilization of functional nano-objects in living engineered bacterial biofilms for catalytic applications, *Natl. Sci. Rev.* 6 (2019) 929–943.
- [54] J.L. Mark Welch, Y. Hasegawa, N.P. McNulty, J.I. Gordon, G.G. Borisy, Spatial organization of a model 15-member human gut microbiota established in gnotobiotic mice, *Proc. Natl. Acad. Sci. U.S.A.* 114 (2017) 9105–9114.
- [55] H.E. Streett, K.M. Kalis, E.T. Papoutsakis, A strongly fluorescing anaerobic reporter and protein-tagging system for *Clostridium* organisms based on the fluorescence-activating and absorption-shifting tag protein (FAST), *Appl. Environ. Microbiol.* 85 (2019) e00622-19.
- [56] T.C. Fung, C.A. Olson, E.Y. Hsiao, Interactions between the microbiota, immune and nervous systems in health and disease, *Nat. Neurosci.* 20 (2017) 145–155.
- [57] Q. Liu, Y. Gai, Y. Chen, X. Lan, D. Jiang, *Escherichia coli* Nissle 1917 as a novel microbot for tumor-targeted imaging and therapy, *Pharmaceutics* 13 (2021) 1226.
- [58] P.F. de Groot, M.N. Frissen, N.C. de Clercq, M. Nieuwdorp, Fecal microbiota transplantation in metabolic syndrome: history, present and future, *Gut Microb.* 8 (2017) 253–267.
- [59] E.N. Baruch, I. Youngster, G. Ben-Betzalel, R. Ortenberg, A. Lahat, L. Katz, K. Adler, D. Dick-Necula, S. Raskin, N. Bloch, D. Rotin, L. Anafi, C. Avivi, J. Melnichenko, Y. Steinberg-Silman, R. Mamtani, H. Harati, N. Asher, R. Shapira-Frommer, T. Brosh-Nissimov, Y. Eshet, S. Ben-Simon, O. Ziv, M.A.W. Khan, M. Amit, N.J. Ajami, I. Barshack, J. Schachter, J.A. Wargo, O. Koren, G. Markel, B. Boursi, Fecal microbiota transplant promotes response in immunotherapy-refractory melanoma patients, *Science* 371 (2021) 602–609.
- [60] Q. Song, C. Zheng, J. Jia, H. Zhao, Q. Feng, H. Zhang, L. Wang, Z. Zhang, Y. Zhang, A probiotic spore-based oral autonomous nanoparticles generator for cancer therapy, *Adv. Mater.* 31 (2019) e1903793.